

PCCP

Accepted Manuscript



This is an *Accepted Manuscript*, which has been through the Royal Society of Chemistry peer review process and has been accepted for publication.

Accepted Manuscripts are published online shortly after acceptance, before technical editing, formatting and proof reading. Using this free service, authors can make their results available to the community, in citable form, before we publish the edited article. We will replace this *Accepted Manuscript* with the edited and formatted *Advance Article* as soon as it is available.

You can find more information about *Accepted Manuscripts* in the [Information for Authors](#).

Please note that technical editing may introduce minor changes to the text and/or graphics, which may alter content. The journal's standard [Terms & Conditions](#) and the [Ethical guidelines](#) still apply. In no event shall the Royal Society of Chemistry be held responsible for any errors or omissions in this *Accepted Manuscript* or any consequences arising from the use of any information it contains.

ARTICLE

A Systematic Study of Metal-Supported Boron Nitride Materials for the Oxygen Reduction Reaction

Cite this: DOI: 10.1039/x0xx00000x

Ralph Koitz,^a Jens K. Nørskov,^b and Felix Studt^{b*}Received 00th January 2012,
Accepted 00th January 2012

DOI: 10.1039/x0xx00000x

www.rsc.org/

Surfaces that efficiently catalyse the oxygen reduction reaction (ORR) are highly desirable for applications in energy utilization. Here, we computationally investigate the ORR on hexagonal boron nitride (*h*-BN) supported on Ni, Cu, and Co. We find a significant influence of the metal on the reaction energetics. In particular, *h*-BN/Cu is predicted to catalyse the ORR with a low overpotential, while on the other substrates the reaction is impeded by the formation of too stable surface hydroxyl species. Our results highlight trends in the reactivity of these heterostructures and may guide further rational design of O₂-activating catalysts based on supported *h*-BN.

Introduction

Fuel cell technology is one of the most promising options for sustainable power generation in the transportation sector beyond fossil fuels.¹ One of the key processes in a fuel cell is the electrochemical reduction of O₂ to H₂O, the so-called oxygen reduction reaction (ORR). In order to make this 4-electron, 4-proton process practically viable, suitable catalysts have to be employed that are efficient, stable and cost-effective.² Currently, the most efficient catalysts contain expensive and scarce metals such as palladium and platinum.³⁻⁴ Alloying of Pd and Pt with non-precious metals has been shown to reduce the overpotential necessary to drive this reaction while at the same time reducing the amount of precious metals.⁵⁻¹⁰ Yet, even for the best materials both overpotential and precious metal content are still significantly calling for alternative catalysts that are either metal-free or based on abundant transition metals.

Two-dimensional materials such as graphene¹¹⁻²⁰ and hexagonal boron nitride (*h*-BN)^{21,22} have recently emerged as promising candidates for the ORR. These materials can be prepared as free-standing sheets but can also be supported on transition metal surfaces. *h*-BN (Fig. 1(a)), in particular is a chemically robust wide-gap semiconductor²³ that has been successfully prepared on numerous substrates (Ni, Cu, Rh, Ru, Fe, Co, Ir, etc.), giving rise to versatile and functional heterostructures (Fig. 1(b)).²³⁻³⁸ Recent work suggests that *h*-BN/metal combinations, particularly *h*-BN/Ni(111) may favourably adsorb and activate molecular O₂,³⁹ and *h*-BN/Au(111) has in fact been shown to be active for the ORR.²² This class of materials has thus the potential to be an alternative to current precious-metal ORR catalysts.

Herein, we examine the thermodynamics of the ORR of *h*-BN supported on non-precious metal surfaces. We focus on Ni(111), Cu(111) and Co(0001) as these surfaces have the smallest lattice mismatch when compared to *h*-BN.⁴⁰ In the first

section we briefly summarize the properties of the bare *h*-BN/metal heterostructures. Subsequently we quantify the free energy profile of the various ORR intermediates on the three supported systems and calculate the theoretical overpotentials necessary to drive the ORR. Finally, we analyse the data to investigate trends and correlations within this class of materials that point towards the properties an optimal material should have.

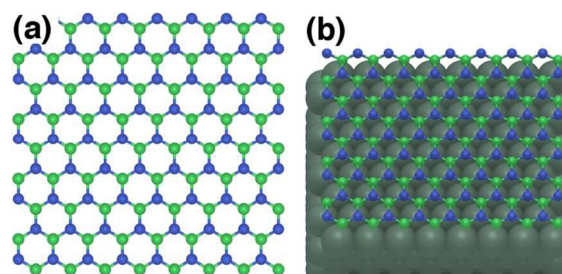


Figure 1. (a) Sketch of an *h*-BN sheet (b) *h*-BN sheet adsorbed on a metal surface. Color codes: N: blue, B: green, Metal: grey-green

Computational Details

For all calculations we employ the Atomic Simulation Environment (ASE)⁴¹ in connection with the QUANTUM ESPRESSO⁴² program package. The electronic wavefunctions are expanded in plane waves up to a cutoff energy of 500 eV, while the electron density is represented on a grid with an energy cutoff of 5000 eV. Core electrons are approximated with ultrasoft pseudopotentials.⁴³ We use the BEEF-vdW exchange-correlation functional,⁴⁴ that has been shown to accurately describe chemisorption as well as physisorption properties on transition metal surfaces.⁴⁵ BEEF-vdW, the “Bayesian Error

Estimation Functional” with van der Waals corrections is a recent addition to the multitude of available XC functionals with several key improvements. The correlation contribution is composed of LDA and PBE correlation in a ratio of approx. 60:40. The exchange energy is modelled in a basis of very flexible functions, which are fitted to an extensive data set with an emphasis on surface science reference data. The vdW-DF2⁴⁶ functional is used to compute non-local correlation energies. Due to the unique machine learning-based fitting approach, the BEEF-vdW functional can be used to calculate uncertainties in the calculated energies based on an error ensemble.⁴⁴

Free energy corrections for adsorbed species are based on the harmonic approximation and calculated vibrational frequencies. We use a corrected total energy for gas-phase O₂ based on the formation enthalpy of H₂O as described previously.⁴⁷ BN/metal surfaces are modelled as slabs with 4 layers of metal (the bottom two layers are fixed at bulk atomic positions), one layer of *h*-BN, and adsorbed species atop *h*-BN. In order to achieve commensurate adsorption, the BN layer is fitted to match the surface lattice constant of the metal and used as a reference for adsorption energy calculations. A vacuum region of about 20 Å is used to decouple the periodic replicas. For adsorption studies we generally use supercells of lateral size 3x3, and sample the Brillouin zone⁴⁸ with a mesh of 4x4x1 k-points. We estimate the uncertainty of the presented DFT energies through an ensemble of exchange-correlation functionals representing the known computational errors of the BEEF-vdW functional as reported elsewhere.⁴⁹

Results and Discussion

Properties of the *h*-BN/Metal Heterostructures

Numerous computational and experimental studies have examined the properties of *h*-BN adsorbed on various metal surfaces.^{23,24,27,37,38,40,50-56} For this reason we only briefly summarize our results obtained for *h*-BN supported on Ni(111), Co(0001) and Cu(111) with the BEEF-vdW functional, which are largely in line with previous experimental and theoretical reports.^{24,32,34,39,40,50-56} Two factors govern the interaction between *h*-BN and the substrate: their lattice mismatch and the strength of their interaction.^{40,50} Ni, Co, and Cu all have small mismatches with *h*-BN ranging from 0.4% to -2.2%, leading to commensurate adsorption. Laterally, the *h*-BN layer can be placed in six high-symmetry adsorption registries, with N or B in *top*, *hcp*, and *fcc* sites, respectively, giving rise to the combinations N_{top}B_{fcc}, N_{top}B_{hcp}, N_{fcc}B_{hcp}, B_{top}N_{hcp}, B_{top}N_{fcc}, B_{fcc}N_{hcp}. The adsorption energies (ΔE_{ads}), BN-metal distances ($d_{\text{BN-M}}$) and vertical B-N buckling ($d_{\text{B-N}}$) for the three substrates in six registries are given in Table 1. For comparison, we show the interaction energies ΔE_{int} in Table S1 of the supporting information. Differences to ΔE_{ads} are small in magnitude so that the general trends are preserved. Our results indicate that *h*-BN binds either as a *physisorbed* or *chemisorbed* layer. The former is characterized by BN-metal distances > 3.4 Å and negligible B-N buckling, while the latter exhibits $d_{\text{BN-M}} < 2.3$ Å and $d_{\text{B-N}} \approx 0.1$ Å. The chemisorbed configurations are higher in energy than the physisorbed ones. This has been observed previously when employing GGA functionals.⁵² A possible cause for this is an over-stabilization of bonds within the BN sheet, leading to energetic penalties for the buckling associated with chemisorption. E.g. the energy required for the buckling of *h*-

BN when adsorbed on Ni(111) amounts to about 60 meV, which essentially accounts for the observed energy difference.

Table 1. Adsorption Energies per BN pair (ΔE_{ads} , eV), BN-Metal distances ($d_{\text{BN-M}}$, Å) and vertical B-N buckling ($d_{\text{B-N}}$, Å) for *h*-BN on Ni(111), Cu(111) and Co(0001) in 6 adsorption registries. The indicated uncertainty is derived using the BEEF-vdW ensemble of exchange-correlation functionals.

	Ni(111)	Cu(111)	Co(0001)	
ΔE_{ads}	N _{top} B _{fcc}	-0.005±0.102	-0.079±0.029	-0.115±0.136
	N _{top} B _{hcp}	0.001±0.088	-0.080±0.027	-0.100±0.136
	N _{fcc} B _{hcp}	-0.079±0.021	-0.077±0.024	-0.082±0.022
	B _{top} N _{fcc}	-0.079±0.022	-0.076±0.025	-0.082±0.021
	B _{top} N _{hcp}	-0.078±0.023	-0.075±0.025	-0.081±0.021
	B _{fcc} N _{hcp}	-0.079±0.019	-0.076±0.023	-0.082±0.022
$d_{\text{BN-M}}$	N _{top} B _{fcc}	2.19	3.43	2.03
	N _{top} B _{hcp}	2.26	3.50	2.04
	N _{fcc} B _{hcp}	3.70	3.82	3.89
	B _{top} N _{fcc}	3.70	3.74	3.90
	B _{top} N _{hcp}	3.62	3.78	3.90
	B _{fcc} N _{hcp}	3.75	3.82	3.81
$d_{\text{B-N}}$	N _{top} B _{fcc}	0.087	0.006	0.126
	N _{top} B _{hcp}	0.076	0.004	0.127
	N _{fcc} B _{hcp}	0.002	0.001	0.001
	B _{top} N _{fcc}	0.002	0.002	0.001
	B _{top} N _{hcp}	0.003	0.001	0.001
	B _{fcc} N _{hcp}	0.001	0.001	0.002

Ni(111) and Co(0001) give rise to chemisorbed heterostructures when *h*-BN is placed with N atoms atop the metal sites, and physisorbed systems in all other cases. Conversely, Cu(111) only weakly interacts with *h*-BN, yielding physisorption for all lateral positions of the sheet. The weakly bound configurations are characterized by $d_{\text{BN-M}}$ typically in the range 3.6-3.8 Å, independent of the metal and adsorption registry. We rationalize this with the largely unspecific dispersive interactions that govern this regime. $d_{\text{BN-M}}$ is slightly smaller for *h*-BN in N_{top} configurations on Cu(111). Experimental LEED studies have found N_{top}B_{fcc} to be the preferred registry of *h*-BN/Ni(111), with a $d_{\text{N-Ni}}$ of 2.22 Å and a B-N buckling of 0.18 Å.³² Related XPD studies found $d_{\text{N-Ni}} = 1.95 \pm 0.16$ Å³¹ and a $d_{\text{B-N}} = 0.07 \pm 0.06$ Å.³⁴ The strong interaction of *h*-BN with Ni(111)²³ and its much weaker interaction with Cu(111)^{23,24} are also in agreement with the available experimental evidence. For *h*-BN/Cu(111) ΔE_{ads} was determined as -59.7 meV per unit cell from scanning tunneling spectroscopy, in good agreement with our calculations.²⁴ Experimental data on *h*-BN/Co(0001) are scarce, but the material has been successfully prepared, observing commensurate adsorption in N_{top}B_{fcc} and N_{top}B_{hcp} registries, in accordance with our results.²⁶

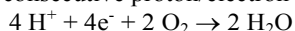
The errors in ΔE_{ads} as obtained from the BEEF-vdW ensembles are on the order of 20 meV for the physisorbed structures, and 88-136 meV for the chemisorbed systems. Relative to the small energies, this confidence interval is of appreciable magnitude, but the absolute error in energy is roughly what can be expected from DFT calculations. The considerable widening of the error bars for chemisorbed heterostructures has been observed before on the example of graphene on Ni(111).⁴⁴

Previous results for adsorption energies of *h*-BN on transition metals vary rather widely, depending on the employed

functional and applied dispersion corrections.⁵⁰ ΔE_{ads} ranges from -0.39^{50} to $+0.04^{52}$ eV for *h*-BN/Ni, from -0.27^{50} to $+0.01^{40}$ eV for *h*-BN/Cu, and from -0.73^{55} to $+0.29^{56}$ for *h*-BN/Co. For all three metals, our results are within the reported ranges. The adsorption energies of the physisorbed configurations are similar for all three metals, indicative of the predominantly dispersive and unspecific nature of binding. For Co(0001), the expected trend that chemisorbed species should have a higher binding energy is fulfilled. E_{ads} on Co(0001) is the largest among the examined metals. As the $N_{\text{top}}B_{\text{fcc}}$ registry is generally the most stable chemisorbed one, and for comparability with previous work, all subsequent calculations are carried out with that adsorption configuration.

Energetics of the ORR on metal-supported *h*-BN

We now employ DFT calculations to elucidate the reaction mechanism of the ORR. The ORR proceeds through four consecutive proton/electron transfer steps



via the intermediates OOH*, O*, OH*. Here, the * indicates adsorbed intermediates. This reaction can be modelled using the computational hydrogen electrode (CHE) that is described elsewhere.⁵⁷ The CHE has been successfully applied to the ORR on transition metals,⁵⁷ transition-metal oxides,⁵⁸ and doped carbon materials⁵⁹ as well as for other electrochemical processes like CO₂ and N₂ reduction.^{60,61} Within this model, zero voltage is defined based on the reversible hydrogen electrode where the protons and electrons are in equilibrium with gas-phase H₂ so that the chemical potential of a proton/electron pair equals $\frac{1}{2}\text{H}_2(\text{g})$. The influence of the applied potential can then be calculated by

$$\Delta G = -eU$$

where e is the number of transferred electrons and U is the applied potential.⁵⁷

We calculated the free energies at 298 K for these adsorbates on all 3 *h*-BN/metal substrates. The ideal ORR catalyst should exhibit a free energy difference as close as possible to the reversible potential of the ORR, -1.23 V, between each intermediate step as deviations from this ideal behaviour lead to an overpotential for this reaction.

ORR on *h*-BN/Ni(111) and *h*-BN/Co(0001)—*h*-BN itself is rather unreactive,^{35,53} but can be made reactive when supported on transition metal surfaces.⁵⁴ The activity of unsupported *h*-BN for the ORR is hence very low as manifested by the very low binding energies of OOH, O, and OH (see Figure S1 in supporting information). When supported on transition metals, however, the electronic structure of *h*-BN changes, making it much more active. Specifically, partial metallization of the BN layer has been noted,⁵⁴ as well as a change of the work function.²⁴ Furthermore, structural effects such as buckling of adsorbed *h*-BN likely also affect its reactivity. We tested the activity of supported *h*-BN towards the ORR on Ni(111), Co(0001) and Cu(111). The optimized structures of the three intermediates for the ORR on *h*-BN/Ni(111) and *h*-BN/Co(0001) are shown in Figure 2, along with a reaction profile at $U=0$ V (Table S2 of the supporting information shows the specific entropy contributions to the free energies shown here). On *h*-BN/Ni(111), the first intermediate, OOH*, is bound to a B atom with a bond length of 1.48 Å, equal to the O-O distance. The O-O bond points away from the surface plane at an angle of about 39° . The O-O bond is stretched ($d_{\text{O-O}}=1.49$ Å), resembling a peroxy species. The B atom bound to O is

displaced from the *h*-BN plane by about 0.5 Å, stretching the corresponding B-N bonds by about 0.07 Å (4.8%). The second intermediate, O*, is located directly above a surface B atom, at a distance somewhat shorter than for OOH*. Here, B is slightly farther from the BN layer (0.6 Å). Finally, the OH* species exhibits $d_{\text{B-O}}$ and $d_{\text{O-H}}$ bond lengths similar to those in OOH*. These structural results are in good agreement with previous theoretical analyses.⁵⁴

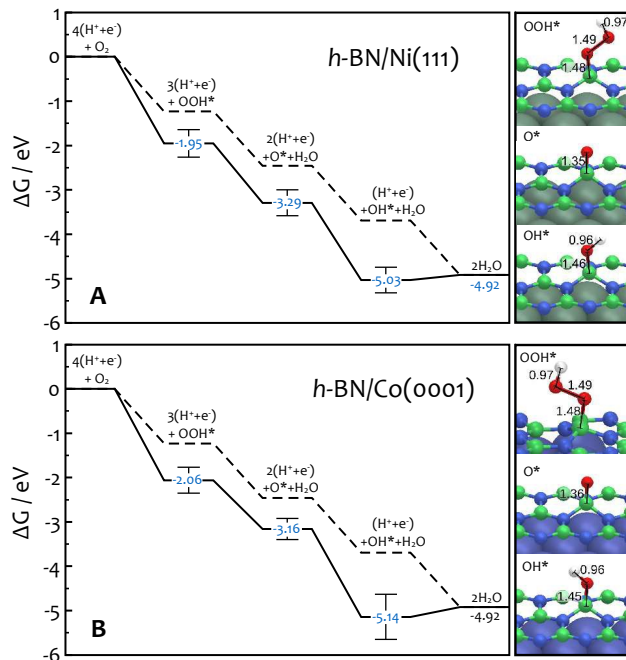


Figure 2. Energy profile of the ORR and optimized structures of OOH*, O* and OH* intermediates on (A) *h*-BN/Ni(111) and (B) *h*-BN/Co(0001). Solid lines show calculated values, dashed lines indicate the energy profile of an ideal ORR catalyst. All distances in Å. N is blue, C is green, O is red and H is white. Error bars are obtained using the BEEF-vdW ensemble of exchange-correlation functionals.

Without an external potential the first step, $\text{O}_2(\text{g}) + \frac{1}{2}\text{H}_2 \rightarrow \text{OOH}^*$ is downhill in free energy by -1.95 eV, noticeably more than for the ideal ORR catalyst (see dashed line in Figure 1). The following reduction of OOH* to O* (while releasing an H₂O molecule) is exothermic by -1.34 eV. The third step, $\text{O}^* + \frac{1}{2}\text{H}_2 \rightarrow \text{OH}^*$ is downhill by -1.94 eV, reaching a minimum of -5.03 eV relative to gas-phase O₂, lower than the overall free energy of the ORR. Adsorbed OH* on *h*-BN/Ni thus constitutes a thermodynamic sink that would prevent the reaction from continuing. This result is in line with previous findings that indicate a too strong adsorption of OH* on *h*-BN/Ni.⁵⁴ ORR on *h*-BN/Co(0001) is very similar to *h*-BN/Ni(111) (see figure 1b). The interatomic distances of the adsorbed species are very similar to those on *h*-BN/Ni and the reaction profile is qualitatively the same as that observed on *h*-BN/Ni(111). At $U=0$ V the first step is downhill in free energy by -2.06 eV, followed by the O* intermediate at -3.16 eV and OH* at -5.14 eV. As for *h*-BN/Ni, the OH* species is bound too strongly for the ORR to proceed.

Generally, it appears that *h*-BN/Co is comparable to *h*-BN/Ni as an ORR catalyst, with only minor quantitative differences in the thermodynamics. Thus, it appears that the Co(0001) substrate is equally able to activate the boron nitride overlayer, but also

results in overall too strong adsorption relative to the ideal behaviour of an ORR catalyst.

ORR on *h*-BN/Cu(111) — Figure 3 shows the optimized structures of ORR intermediates on *h*-BN/Cu. In all cases, the bond lengths and adsorption distances are very similar to those found on *h*-BN/Ni(111) and *h*-BN/Co(0001). The O* species is adsorbed noticeably closer to the surface (1.35 Å) than the others and the O-O bond length in OOH* is equally long as the O-B bond length in the same species. Again, the B atom binding the adsorbate is slightly displaced out of the *h*-BN plane in all cases.

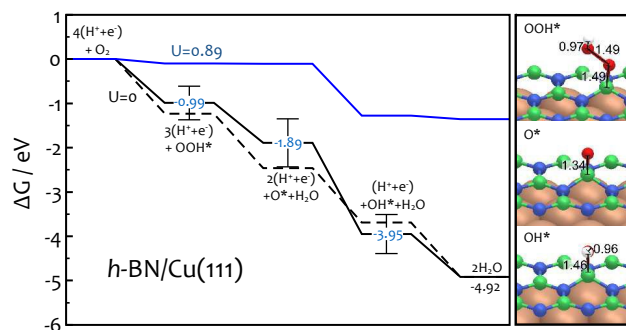


Figure 3. Energy profile of the ORR and optimized structures of OOH*, O* and OH* intermediates on *h*-BN/Cu(111). Solid lines show calculated values, dashed lines indicate the energy profile of an ideal ORR catalyst. All distances in Å. N is blue, C is green, O is red and H is white. Error bars are obtained using the BEEF-vdW ensemble of exchange-correlation functionals.

Figure 3 shows the free energy diagram for the ORR on *h*-BN/Cu(111). In addition to the free energy profile at $U=0$ we also show the maximum potential at which all steps of this reaction are still downhill in energy, which is 0.89 V. Without an external potential, the OOH* species is bound with a ΔG of -0.99 eV, O* with -1.89 eV and OH* with -3.95 eV. Compared to *h*-BN/Ni(111) and *h*-BN/Co(0001), all intermediates are bound less strongly by at least 1 eV, which significantly changes the overall profile of the reaction. Notably, the energy difference between each step is much closer to the ideal 1.23 eV. All steps are exothermic up to an external potential of $U=0.89$ V, yielding the overpotential 0.34 V, which is somewhat lower than the theoretical value for the ORR on Pt(111).⁵⁷ Importantly, the free energy difference between OOH* and OH* is about 3 eV which is close to values found for transition metals⁴⁷ and transition metal oxides.⁶² We used the BEEF-vdW ensemble to provide a measure of confidence for the predicted ORR activity of *h*-BN/Cu(111), the result of which is shown in Figure 4. Here we show the probability with which *h*-BN/Cu(111) is predicted to have a certain overpotential for ORR. While there is a certain distribution related to the uncertainty of the DFT calculations, we note that there is an almost 50% probability that the ORR overpotential is smaller than 0.5 V, and 84% probability that it is smaller than 0.7 V.

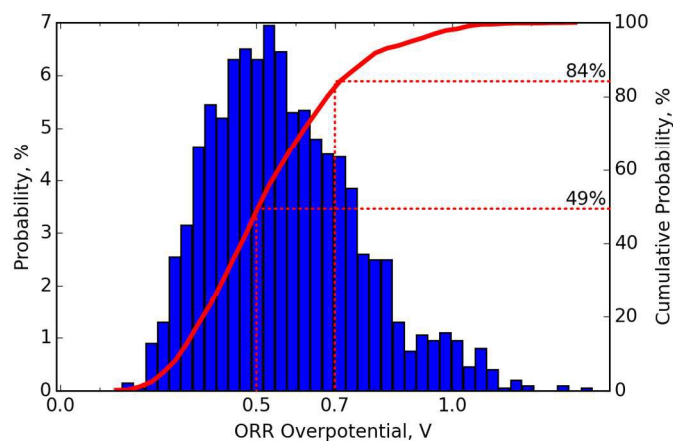


Figure 4. Histogram of theoretically predicted overpotentials for the ORR on *h*-BN/Cu(111) using the BEEF-vdW ensemble of exchange-correlation functionals. The red curve indicates the cumulative probability (right y axis), with the overpotential being smaller than 0.5 V (0.7 V) having a probability of 49% (84%).

The influence of the in-plane lattice constant on the ORR on *h*-BN/Ni(111) - In order to elucidate the influence of the metal-metal bonding on the ORR, we artificially expanded the Ni surface laterally by a strain factor $\alpha = 2, 4,$ and 6%. Note that applying compressive strain (as small as 1%) led to the detachment of the *h*-BN layer from the metal surface, i.e. breakdown of the chemisorbed heterostructure.

Table 2 lists the free energies of the ORR intermediates at the different degrees of strain. $\Delta G(\text{OOH}^*)$ is largely independent of the strain, remaining near the $\alpha = 0$ value (-1.95 eV). $\Delta G(\text{OH}^*)$ also shows little variation with α , decreasing slightly from -5.03 to -5.12 eV as α is increased to 2%, then remaining the same. We find the stretching of the lattice constant to have the greatest effect on $\Delta G(\text{O}^*)$, which is stabilized by 0.16 eV at $\alpha=6\%$, following an approximately linear trend. However, also this effect is rather minor, considering that a strain of 6% corresponds to an increase of the in-plane interatomic distances by 0.15 Å. The approach of stretching the material allows for some control over the intermediates' binding energies, but tends to stabilize rather than destabilize them as would be desirable for improving the ORR.

Table 2. Influence of strain on the free energy of ORR intermediates on *h*-BN/Ni(111) at various degrees of lateral expansion of the substrate lattice constant. All energies in eV and relative to $\text{O}_2(\text{g})$ and 4 proton-electron pairs as in Figure 2.

strain, %	$\Delta G(\text{OOH}^*)$	$\Delta G(\text{O}^*)$	$\Delta G(\text{OH}^*)$
0.0	-1.95	-3.29	-5.03
2.0	-1.99	-3.37	-5.12
4.0	-1.97	-3.39	-5.10
6.0	-1.97	-3.45	-5.10

Trends in adsorption energetics and reactivity

We will now try to identify trends that might allow one to optimize the catalyst materials. In the context of the O_2 evolution reaction it was found that materials generally obey the relation $\Delta G(\text{OOH}^*) - \Delta G(\text{OH}^*) = 3.2$ eV.⁶² When comparing our data we find an average difference $\Delta G(\text{OOH}^*) - \Delta G(\text{OH}^*)$ of 3.09 eV for the various materials, being largely in line with what is observed for transition

metals⁴⁷ and oxides.⁶² Due to the limited data we refrain from establishing linear relations but we note that the fairly large gap between *h*-BN/Cu(111) and the other data points suggest that a number of materials with intermediate values of ΔG might still be found.

Conclusions

In this article we presented a comprehensive study of three metal-supported *h*-BN materials, *h*-BN/Ni(111), *h*-BN/Cu(111) and *h*-BN/Co(0001) in the context of their activity towards the ORR. Concerning the structures of adsorbates and intermediates, all substrates are similar and the results are within the expected ranges. We determined free-energy diagrams for all steps of the ORR on these substrates. OH* species tend to be too strongly bound on *h*-BN/Ni and *h*-BN/Co, leading us to conclude that these materials are unlikely to be efficient ORR catalysts in practice. Inducing an artificial lateral strain in *h*-BN/Ni has little effect on the free energies of adsorbed species. In contrast, overall adsorption free energies on *h*-BN/Cu are smaller, leading to more favourable energy differences between the ORR steps. We calculate an overpotential of 0.34 eV, comparable to that of the ORR on Pt(111). We note here, however, that solvation effects by the water layer at the water-solid interface are not included in the present analysis. These effects have been shown to be as large as 0.25 and 0.5 eV for OOH* and OH*, respectively.^{57,63,64} If similar corrections are needed for supported *h*-BN, the theoretical overpotential for *h*-BN/Cu(111) would increase to 0.59 V (a histogram of the theoretically predicted overpotentials applying this correction and using the BEEF-vdW ensemble of exchange-correlation functionals is shown in the SI). Similarly, the difference between $\Delta G(\text{OOH}^*)$ and $\Delta G(\text{OH}^*)$ would increase to ~ 3.21 eV. Further studies on the effect of solvation on the free energy profile are hence needed in order to establish the magnitude of these solvation effects. In summary, our study shows that metal-supported *h*-BN exhibits tunable ORR performance depending on the metal employed, and that *h*-BN/Cu is a promising substrate for catalysing the ORR. Further studies in this direction are likely to be rewarding, both in the context of experimental verification of these results, as well as the further exploration of related metal-monolayer heterostructures.

Acknowledgements

RK thanks the Swiss National Science Foundation for funding under grant no 20021_140441. F.S. and J.K.N gratefully acknowledge support from the U.S. Department of Energy, Office of Sciences, Office of Basic Energy Sciences to the SUNCAT Center for Interface Science and Catalysis.

Notes and references

- G. Crabtree, and M. Dresselhaus, *MRS Bulletin*, 2008, **33**, 421.
- A. Morozan, B. Joussemme and S. Palacin, *Energy Environ. Sci.*, 2011, **4**, 1238.
- Y. Tan, C. Xu, G. Chen, N. Zheng and Q. Xie, *Energy Environ. Sci.*, 2012, **5**, 6923
- D. J. Berger, *Science*, 1999, **286**, 5437

- V.R. Stamenkovic, B. Fowler, B. S. Mun, G. W. Wang, P. N. Ross, C. A. Lucas, N. M. Markovic, *Science*, 2007, **315**, 493.
- M. Lefevre, E. Proietti, F. Jaouen, J. P. Dodelet, *Science*, 2009, **324**, 71.
- J. Greeley, I. E. L. Stephens, A. S. Bondarenko, T. P. Johansson, H. A. Hansen, T. F. Jaramillo, J. Rossmeisl, I. Chorkendorff, J. K. Nørskov, *Nat. Chem*, 2009, **1**, 552.
- C. Wang, D. Li, M. Chi, J. Pearson, R. B. Rankin, J. Greeley, Z. Duan, G. Wang, D. van der Vliet, K. L. More, N. M. Markovic, V. R. Stamenkovic, *J. Phys. Chem. Lett.*, 2012, **3**, 1668.
- C. Wang, N. M. Markovic, V. R. Stamenkovic, *ACS Catal.*, 2012, **2**, 891.
- P. Hernandez-Fernandez, F. Masini, D. N. McCarthy, C. E. Strebler, D. Friebe, D. Deiana, P. Malacrida, A. Nierhoff, A. Bodin, A. M. Wise, J. H. Nielsen, T. W. Hansen, A. Nilsson, I. E. L. Stephens, I. Chorkendorff, *Nature Chem.* 2014, **6**, 732.
- K. Gong, F. Du, Z. Xia, M. Durstock, L. Dai, *Science*, 2009, **323**, 760
- R. Liu, D. Q. Wu, X. L. Feng, K. Müllen, *Angew. Chem. Int. Ed.*, 2010, **49**, 2565.
- L. Qu, Y. Liu, J.-B. Baek, L. Dai, *ACS Nano*, 2010, **4**, 1321.
- S. Yang, X. Feng, X. Wang, K. Müllen, *Angew. Chem. Int. Ed.*, 2011, **50**, 5339.
- D. Yu, E. Nagelli, F. Du, L. Dai, *J. Phys. Chem. Lett.* 2010, **1**, 2165.
- Z.-W. Liu, F. Peng, H.-J. Wang, H. Yu, W.-X. Zheng, J. Yang, *Angew. Chem. Int. Ed.* 2011, **50**, 3257.
- D. S. Su, S. Perathoner, and G. Centi, *Chem. Rev.*, 2013, **113**, 5782.
- W. Yang, T.-P. Feller, M. Antonietti, *J. Am. Chem. Soc.*, 2011, **133**, 206.
- J. Benson, Q. Xu, P. Wang, Y. Shen, L. Sun, T. Wang, M. Li and P. Papakonstantinou, *ACS Appl. Mater. Interfaces*, 2014, **6**, 19726.
- Y. Li, M. Li, L. Jiang, L. Lin, L. Cui and X. He, *Phys. Chem. Chem. Phys.*, 2014, **16**, 23196–23205.
- S. Wang, L. Zhang, Z. Xia, A. Roy, D. W. Chang, J.-B. Baek, and L. Dai, *Angew. Chem. Int. Ed.*, 2012, **51**, 4209
- K. Uosaki, G. Elumalai, H. Noguchi, T. Masuda, A. Lyalin, A. Nakayama, and T. Taketsugu, *J. Am. Chem. Soc.*, 2014, **136**, 6542.
- A. B. Preobrajenski, A. S. Vinogradov and N. Martensson, *Surf. Sci.*, 2005, **582**, 21–30.
- S. Joshi, D. Eciya, R. Koitz, M. Iannuzzi, A.P. Seitsonen, J. Hutter, H. Sachdev, S. Vijayaraghavan, F. Bischoff, K. Seufert, J. V. Barth, and W. Auwärter, *Nano Lett.*, 2012, **12**, 5821.
- M. Corso, W. Auwärter, M. Muntwiler, A. Tamai, T. Greber, and J. Osterwalder, *Science*, 2004, **303**, 217.
- C. Orofeo, S. Suzuki, H. Kageshima, and H. Hibino, *Nano Res.*, 2013, **6**, 335
- B. Wang and M.-L. Bocquet, *J. Phys. Chem. Lett.*, 2011, **2**, 2341–2345.
- H. Cun, M. Iannuzzi, A. Hemmi, J. Osterwalder and T. Greber, *ACS Nano*, 2014, **8**, 7423–31.
- H. Cun, M. Iannuzzi, A. Hemmi, S. Roth, J. Osterwalder and T. Greber, *Nano Lett*, 2013, **13**, 2098–103.
- A. Goriachko, Y. He, M. Knapp, H. Over, M. Corso, T. Brugger, S. Berner, J. Osterwalder and T. Greber, *Langmuir*, 2007, **23**, 2928–31.
- M. Muntwiler, W. Auwärter, F. Baumberger, M. Hoesch and T. Greber, *Surf. Sci.*, 2001, **472**, 125–132.
- Y. Gamou, M. Terai, A. Nagashima and C. Oshima, *Sci. Rep. RITU A44*, 1997, 211–214.

- 33 A. S. Vinogradov, A. A. Zakharov, M. L. Ng, A. Mikkelsen, E. Lundgren, N. Mårtensson and A. B. Preobrajenski, *Langmuir*, 2012, **28**, 1775–81.
- 34 W. Auwärter, T. J. Kreuzer, T. Greber and J. Osterwalder, *Surf. Sci.*, 1999, **429**, 229–236.
- 35 P. Bacle, A. P. Seitsonen, M. Iannuzzi and J. Hutter, *Chimia*, 2014, **68**, 596–601.
- 36 S. Joshi, F. Bischoff, R. Koitz, D. Ecija, K. Seufert, A. P. Seitsonen, J. Hutter, K. Diller, J. I. Urgel, H. Sachdev, J. V. Barth and W. Auwärter, *ACS Nano*, 2013.
- 37 K. K. Kim, A. Hsu, X. Jia, S. M. Kim, Y. Shi, M. Hofmann, D. Nezich, J. F. Rodriguez-Nieva, M. Dresselhaus, T. Palacios and J. Kong, *Nano Lett*, 2012, **12**, 161–6.
- 38 F. Müller, S. Hüfner, H. Sachdev, R. Laskowski, P. Blaha and K. Schwarz, *Phys. Rev. B*, 2010, **82**, 11306.
- 39 A. H. M. A. Wasey, S. Chakrabarty, G. P. Das, and C. Majumder, *ACS Appl. Mater. Interfaces*, 2013, **5**, 10404.
- 40 R. Laskowski, P. Blaha and K. Schwarz, *Phys. Rev. B*, 2008, **78**, 045409.
- 41 S. R. Bahn, K. W. Jacobsen, *Comput. Sci. Eng.*, 2011, **4**, 56.
- 42 P. Giannozzi, S. Baroni, N. Bonini, M. Calandra, R. Car, C. Cavazzoni, D. Ceresoli, G. L. Chiarotti, M. Cococcioni, I. Dabo, A. Dal Corso, S. de Gironcoli, S. Fabris, G. Fratesi, R. Gebauer, U. Gerstmann, C. Gougoussis, A. Kokalj, M. Lazzeri, L. Martin-Samos, N. Marzari, F. Mauri, R. Mazzarello, S. Paolini, A. Pasquarello, L. Paulatto, C. Sbraccia, S. Scandolo, G. Sclauzero, A. P. Seitsonen, A. Smogunov, P. Umari and R. M. Wentzcovitch, *J. Phys. Condens. Matter*, 2009, **21**, 395502.
- 43 A. A. Adllan, A. Dal Corso, *J. Phys. Condens. Matter*, 2011, **23**, 425501.
- 44 J. Wellendorff, K. T. Lundgaard, A. Møgelhøj, V. Petzold, D. D. Landis, J. K. Nørskov, T. Bligaard and K. W. Jacobsen, *Phys. Rev. B*, 2012, **85**, 235149.
- 45 J. Wellendorff, T. L. Silbaugh, D. Garcia-Pintos, J. K. Nørskov, T. Bligaard, F. Studt, C. T. Campbell, *Surf. Sci.*, doi: 10.1016/j.susc.2015.03.023.
- 46 K. Lee, E. D. Murray, L. Kong, B. I. Lundqvist, D. C. Langreth, *Phys. Rev. B*, 2010, **82**, 081101.
- 47 J. Rossmeisl, A. Logadottir and J. K. Nørskov, *Chem. Phys.*, 2005, **319**, 178–184.
- 48 H. J. Monkhorst, J. D. Pack, *Phys. Rev. B*, 1976, **13**, 5188.
- 49 A. J. Medford, J. Wellendorff, A. Vojvodic, F. Studt, F. Abild-Pedersen, K. W. Jacobsen, T. Bligaard, J. K. Nørskov, *Science* 2014, **345**, 197.
- 50 J. Gómez Díaz, Y. Ding, R. Koitz, A. P. Seitsonen, M. Iannuzzi and J. Hutter, *Theor. Chem. Acc.*, 2013, **132**, 1350.
- 51 R. Koitz, A. P. Seitsonen, M. Iannuzzi and J. Hutter, *Nanoscale*, 2013, **5**, 5589–95.
- 52 M. N. Huda and L. Kleinman, *Phys. Rev. B*, 2006, **74**, 075418.
- 53 A. Lyalin, A. Nakayama, K. Uosaki and T. Taketsugu, *Phys. Chem. Chem. Phys.*, 2013, **15**, 2809–20.
- 54 A. Lyalin, A. Nakayama, K. Uosaki, and T. Taketsugu, *J. Phys. Chem. C*, 2013, **117**, 21359.
- 55 N. Joshi and P. Ghosh, *Phys. Rev. B*, 2013, **87**, 235440.
- 56 Y. G. Zhou, X. T. Zu and F. Gao, *Solid State Commun.*, 2011, **151**, 883–886.
- 57 J. K. Nørskov, J. Rossmeisl, A. Logadottir, L. Lindqvist, J. R. Kitchin, T. Bligaard, and H. Jonsson, *J. Phys. Chem. B*, 2004, **108**, 17886–17892.
- 58 J. Rossmeisl, Z. W. Qu, H. Zhu, G. J. Kroes, J. K. Nørskov, *J. Electroanal. Chem.*, 2007, **607**, 83.□
- 59 F. Studt, *Catal. Lett.*, 2012, **143**, 58.
- 60 E. Skúlason, T. Bligaard, S. Gudmundsdóttir, F. Studt, J. Rossmeisl, F. Abild-Pedersen, T. Vegge, H. Jónsson, J. K. Nørskov, *Phys. Chem. Chem. Phys.*, 2012, **14**, 1235.□
- 61 A. A. Peterson, F. Abild-Pedersen, F. Studt, J. Rossmeisl, J. K. Nørskov, *Energy Environ. Sci.* 2010, **3**, 1311.
- 62 I. C. Man, H.-Y. Su, F. Calle-Vallejo, H. A. Hansen, J. I. Martinez, N. G. Inoglu, J. Kitchin, T. F. Jaramillo, J. K. Nørskov, and J. Rossmeisl, *ChemCatChem*, 2011, **3**, 1159–1165.
- 63 V. Tripkovic, E. Skúlason, S. Siahrostami, J. K. Nørskov, J. Rossmeisl, *Electrochim. Acta*, 2010, **55**, 7975.
- 64 G. S. Karlberg, G. Wahnström, *Phys. Rev. Lett.* 2004, **92**, 136103.

^a Department of Chemistry, University of Zurich, Winterthurerstrasse 190, 8057 Zurich, Switzerland

^b SUNCAT Center for Interface Science and Catalysis, SLAC National Accelerator Laboratory, 2575 Sand Hill Road, Menlo Park, CA 94025, USA and Department of Chemical Engineering, Stanford University, Stanford, CA 94305, USA

† Electronic Supplementary Information (ESI) available: [details of any supplementary information available should be included here]. See DOI: 10.1039/b000000x/